Analysis and Mitigation of SSCI when Integrating Wind Power to Series Compensated Lines

I. Löfgren, O. Lennerhag

***Abstract*—As more power electronics are introduced into the power system, its stability is impacted, e.g., through undesired interactions. One such interaction is called sub-synchronous control interaction (SSCI), an example being an interaction between a DFIG wind farm and a series compensated line. In this paper, two methods are used to assess the risk of SSCI: the reactance crossover method, and the Nyquist criterion. The analysis is performed on three case studies: one system based on the IEEE First Benchmark System, and the other system is modelled as a typical Swedish transmission system with two different degrees of series compensation. Both methods predict SSCI in all three case studies, with the Nyquist criterion being able to predict the oscillation frequency more accurately. To mitigate the sub-synchronous oscillations, a PV farm is implemented and placed in parallel to the wind farm. The performed simulations show that it is able to damp the oscillations successfully in all case studies.**

***Keywords*: Nyquist criterion, PV-STATCOM, series compensation, SSCI, SSO, SSR**

I. Introduction

THE amount of electricity generation based on power electronics is increasing and will impact the stability of the power system, e.g., through undesired interactions. TSOs are realizing the importance of this, with e.g., the Swedish TSO Svenska kraftnät seeing further needs to analyze the system impact [1], and the Finnish TSO Fingrid having requirements for the connection of converter-connected power plants close to series compensated systems [2]. One type of interaction which could occur is that between a DFIG based wind farm radially connected to a series compensated line, with the wind farm presenting negative resistance in the sub-synchronous range (i.e., below 50 or 60 Hz) which might lead to sub-synchronous oscillations. This type of interaction is referred to as sub-synchronous control interaction (SSCI) and is the focus of this paper. SSCI is part of the umbrella term sub-synchronous oscillation (SSO), along with sub-synchronous resonance (SSR) and sub-synchronous torsional interaction (SSTI) [3]. SSCI is an interaction between a power electronic control system and a series compensated system, with no mechanical interaction involved. It has been seen in [4] that with a lower active power output reference of a DFIG wind farm, the negative resistance is larger than for higher active power output references. It was also seen that a faster current controller of the DFIG led to more negative resistance.

This paper is based on results of a Master thesis [5] dealing with SSCI between a DFIG wind farm and a series compensated system (modelled as a typical Swedish transmission system). A PV farm is connected in parallel to the wind farm, aiming to mitigate SSCI by acting as a PV-STATCOM. The impedance analysis in this paper is greatly extended from that in [5]. The structure of this paper is as follows: Section II describes the two methods used to analyze the risk of SSCI, Section III describes the case studies and impedance measurement, Section IV describes the implementation of the PV-STATCOM, Section V describes the time domain results, and Section VI describes the frequency domain results. Finally, Section VII and VIII give the discussion and conclusions, respectively.

II. SSCI Risk Analysis

Two methods for assessing the risk of SSCI will be used in this paper, where the first method (further called the reactance crossover method) is that previously used in [5], and the second is the Nyquist criterion. The reactance crossover method, as described in [5], suggests three situations which could imply SSCI and which should be further analyzed using EMT analysis [6]–[8]. The three situations are:

a) $X_{wtg} = 0$ and $X_{grid} = 0$ (reactance crossover on turbine side coinciding with resonant condition on system side)
b) $X_{grid} = 0$ and $R_{wtg} < 0$ (resonant conditions on system side coinciding with negative resistance of turbine)
c) $X_{sum} = 0$ and $R_{sum} < 0$ (reactance crossover combined with negative resistance of total impedance)

The second method, i.e., the Nyquist criterion, uses the open-loop transfer function G_{OL} of the combined system (grid + wind farm) to assess its stability, i.e., the stability of the closed-loop transfer function G_{CL}. By calculating the total impedance as seen from point A in Fig. 1, i.e., by seeing Z_{wtg} and Z_{grid} as parallel impedances, the result is G_{CL} as given in (1), as also in [9].

$$G_{CL}(s) = \frac{Z_{wtg} \cdot Z_{grid}}{Z_{wtg} + Z_{grid}} = \frac{Z_{grid}}{Z_{grid}} \cdot \frac{Z_{wtg}}{\frac{Z_{wtg}}{Z_{grid}} + 1} = \frac{Z_{wtg}}{1 + Z_{wtg} \cdot Y_{grid}} \quad (1)$$

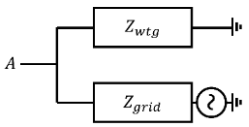

Fig. 1. Wind farm impedance Z_{wtg} and grid impedance Z_{grid}.

I. Löfgren (isabelle@i2g.se) and O. Lennerhag (oscar@i2g.se) are with Independent Insulation Group Sweden AB (I²G), Ludvika, Sweden.

Paper submitted to the International Conference on Power Systems Transients (IPST2023) in Thessaloniki, Greece, June 12-15, 2023.

The corresponding block diagram of G_{CL} is seen in Fig. 2, and the open-loop transfer function G_{OL} is given by (2).

$$C_{OL}(s) = Z_{wtg} \cdot Y_{grid} \tag{2}$$

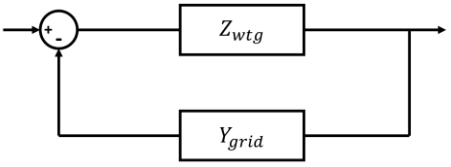

Fig. 2. Block diagram of the closed-loop transfer function $G_{CL}(s)$.

Let P be the number of unstable poles of G_{OL} (or the unstable poles of the characteristic function $1 + G_{OL}$) and let Z be the number of right half-plane (RHP) zeros of the characteristic equation. Let N be the number of clockwise encirclements of the point $-1 + 0j$ of G_{OL}, where $Z = N + P$. The system is stable if $Z = 0$, i.e., $N = -P$ [10]. If the open-loop transfer function G_{OL} is stable, i.e., it has no unstable poles ($P = 0$), the Nyquist criterion simplifies to $Z = N$, i.e., for the closed-loop transfer function G_{CL} to be stable, the open-loop transfer function G_{OL} must not encircle the point $-1 + 0j$. When G_{OL} is stable, it does not encircle the point $-1 + 0j$ if this point lies to the left of the Nyquist diagram of G_{OL} drawn for positive frequencies. Consequently, the point $-1 + 0j$ is encircled by G_{OL} if this point lies to the right of the Nyquist diagram [10]. I.e., if G_{OL} is stable, G_{CL} is stable if $\Re(G_{OL}) > -1$ when $\Im(G_{OL}) = 0$.

III. Case Studies and Impedance Measurement

Two systems were investigated, with the first being a modified version of the IEEE First Benchmark Model (denoted Case A), and the second a representation of a typical Swedish transmission system (denoted Case B).

A. Case Study Systems

The base structure of the two systems is seen in Fig. 3, where no system specific grid parameters are given. The systems are made up of a series compensated line between bus A and WF, and a non-compensated line between bus WF and B. A 200 MW DFIG wind farm is connected to bus WF, using a generic PSCAD DFIG wind farm model documented in [11]. A 200 MW PV farm, described later in this paper, is added in parallel to the wind farm with the aim of damping potential oscillations occurring due to SSCI. The grid parameters of the modified IEEE First Benchmark Model (FBM) system were inspired by those in [4] and are given in [5]. Case A represents a strong grid, where the compensated line had a compensation degree of 20%. The parameters of the Case B system are also given in [5], where line parameters were chosen to represent typical lines used in the Swedish transmission system. The compensated line had a compensation degree of 20% and 50%, for comparison.

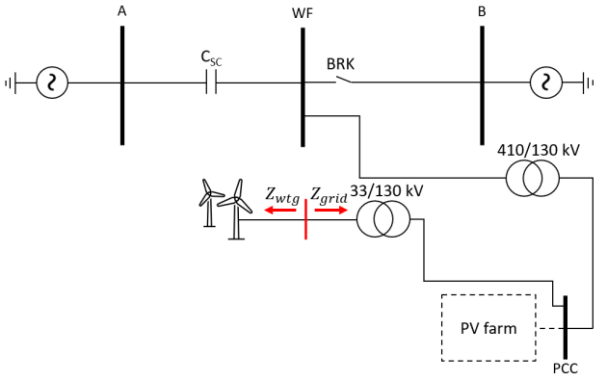

Fig. 3. Base structure of Case A and Case B system (adapted from [5]).

B. Impedance Measurement

The impedance of the grid side of the three case studies, i.e., Z_{grid} in Fig. 3, was measured with the breaker BRK open, and with the wind and PV farms disconnected. Since the grid consisted of passive components only, the built-in frequency scanner module [12] in PSCAD was used to measure Z_{grid}. The wind farm impedance Z_{wtg} was measured using a dynamic impedance scan, since the wind farm is a non-linear system and cannot be measured with a passive impedance scan. The dynamic impedance scan was implemented as in Fig. 4, where a voltage perturbation with the frequency of interest is placed in series with a voltage source of rated system voltage and frequency. The measurement is repeated for each frequency of interest, which in this case was 5-45 Hz in steps of 1 Hz (positive sequence). The amplitude of the voltage perturbation was set to approximately 0.6% of the rated phase-to-neutral voltage.

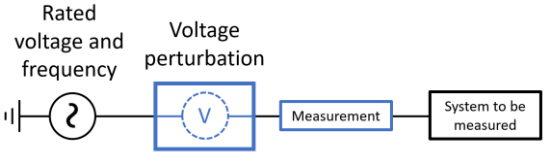

Fig. 4. Series voltage perturbation.

IV. Implementation of PV Farm

An overview of the PV farm model is seen in Fig. 5, and a detailed description of its implementation is given in [5]. The PV modules, producing a maximum of about 202 kW at standard test conditions (STC), are connected to a buck-boost converter which can operate in different modes. The first mode is the maximum power point tracker (MPPT) mode, the second

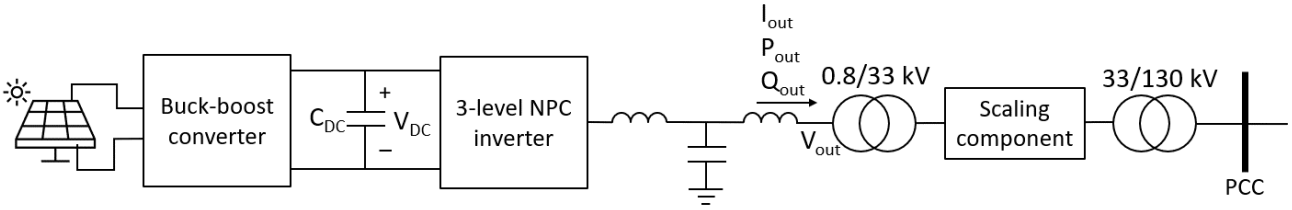

Fig. 5. Overview of PV farm model.

is a fixed active power setpoint, and the third mode disables active power output from the PV to allow for the inverter to be fully utilized as a STATCOM. The inverter model, with specifications based on a 200 kW transformerless three-phase three-level inverter from Huawei [13], was implemented using a neutral-point clamped (NPC) design with space vector modulation (SVM) control. The inverter is connected to a transformer through an LCL filter, the output from the transformer is then scaled by 1000 to model a 200 MW PV farm. Finally, a second transformer connects the PV farm to the point of common coupling (PCC) together with the wind farm.

A. Control System

The PV farm control system consists of an outer DC controller and an inner current controller, further described in [5]. The voltage V_{DC} across the DC link capacitance C_{DC} (see Fig. 5) controls the reference for the d-component (d-axis aligned with phase A) of the current I_{out}, while the reactive power output Q_{out} controls the q-component of I_{out}. The active power output from the PV is controlled by the buck-boost converter, meaning that the outer DC controller should set the d-axis current reference such that the charge balance of C_{DC} is maintained. The control of active and reactive power is decoupled in the inner current control loop which outputs the d and q voltage references for the inverter. The control system, including its tuning, is described in detail in [5].

B. Damping Functionality

The damping functionality was implemented by adjusting the reactive power reference, as seen in Fig. 6. When a sub-synchronous oscillation is detected, the reactive power reference is switched from a fixed value to a damping signal. The damping signal is generated by sending the measured reactive power from the wind farm Q_{wind}, measured at the PCC, through a 5 Hz to 45 Hz bandpass filter, then through a gain block with gain K_d and a delay block.

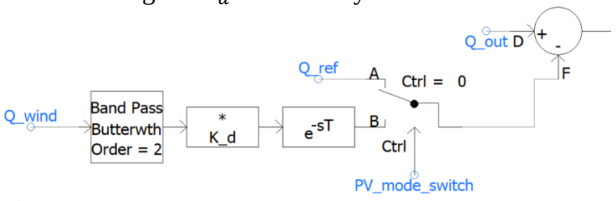

Fig. 6. Generation of damping signal.

The q-component of the voltage at the PCC was used to detect sub-synchronous oscillations, with the complete description of the detection given in [5].

V. Results in Time Domain

Time domain simulations with and without the PV-STATCOM are presented below.

A. Case A

Opening the breaker in Fig. 3 at 1.4 s, leaving the wind farm radially connected to the series compensated grid, resulted in the oscillations seen in Fig. 7 (without damping, in blue) at the PCC (only phase A shown for current and voltage). The current reached values of about 4 p.u, which could cause disconnection or damage to equipment. When the PV-STATCOM is included, it successfully damps the oscillations. Note that prior to the PV farm going into STATCOM mode, the active power at the PCC is twice that without the PV farm (since both the wind farm and PV farm are 200 MW each).

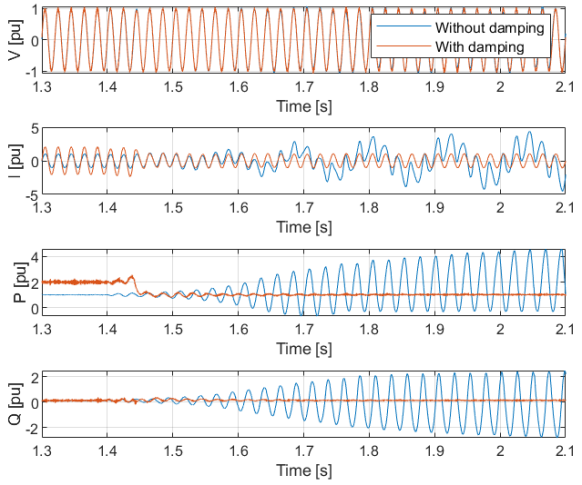

Fig. 7. Case A with 20% compensation, with (red) and without (blue) damping from PV farm (breaker opened at 1.4 s).

The active and reactive power at the PCC before and during the damping, both from the wind farm and PV farm individually, as well as the sum of the two, are seen in Fig. 8. The oscillations have a frequency of about 8-9 Hz (both in phase voltage and current), meaning they are sub-synchronous oscillations. Fast Fourier Transforms (FFTs) of the undamped phase voltage and current are given in Fig. 9.

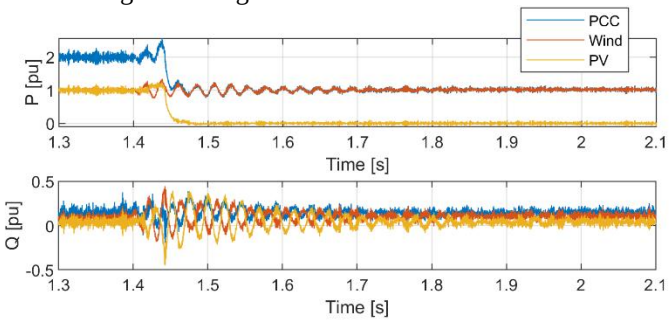

Fig. 8. Case A wind farm, PV, and PCC active and reactive power before and after breaker opening (at 1.4 s) with subsequent damping.

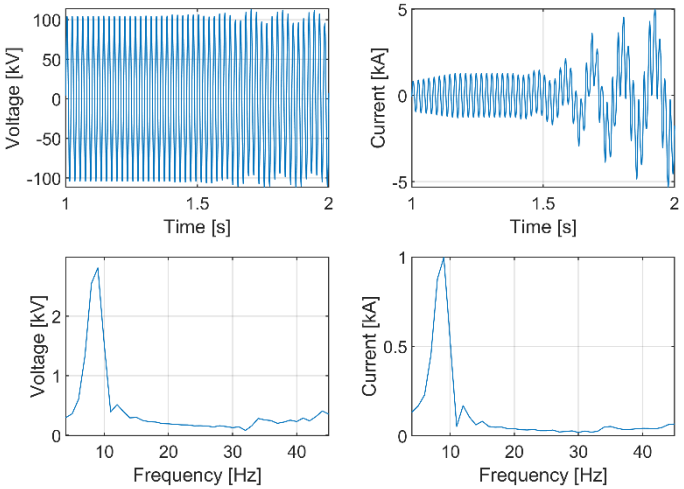

Fig. 9. Waveforms and FFTs of undamped Case A phase voltage (left) and current (right).

B. Case B

Opening the breaker in Fig. 3 at 1.4 s resulted in the waveforms seen in Fig. 10 at the PCC. It is seen that both compensation degrees result in instability, with 50% compensation having oscillations of a higher amplitude than 20% compensation. In both cases, the PV farm successfully damps the oscillations. The frequency of the oscillations (both in phase voltage and current) was about 10-11 Hz with 20% compensation, and about 15 Hz with 50% compensation. FFTs of the undamped phase voltage and current for both compensation degrees are given in Fig. 11. A frequency component of about 9 Hz is also visible in the voltage with 50% compensation, but not in the current.

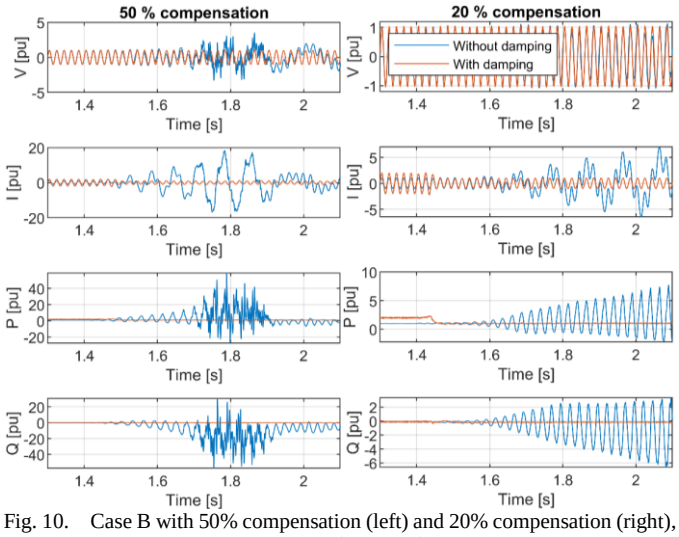

Fig. 10. Case B with 50% compensation (left) and 20% compensation (right), with (red) and without (blue) damping from PV farm (breaker opened at 1.4 s).

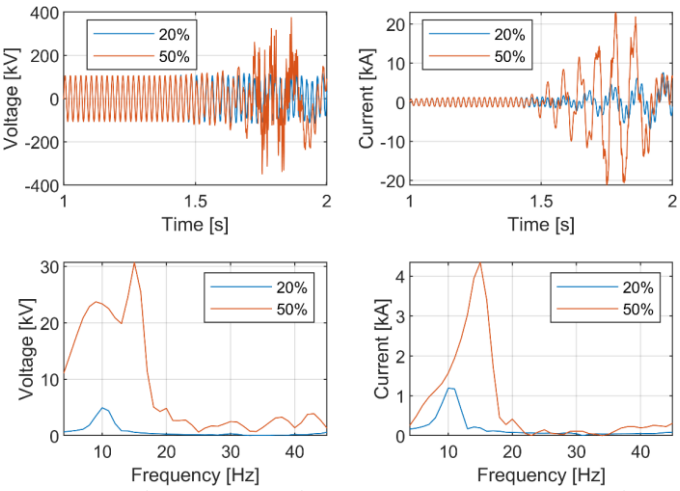

Fig. 11. Waveforms and FFTs of undamped Case B phase voltage (left) and current (right).

VI. Frequency Domain Analysis

The two cases (A and B) are separately analyzed first using the reactance crossover method, followed by the Nyquist criterion.

A. Case A with 20% Compensation

1) Reactance Crossover Criteria

The resistance and reactance of the grid, the wind farm, and the sum of the two are seen in Fig. 12, where the series resonance points are marked with dashed lines. A zoomed in version of the resistances and reactances are seen in Fig. 13. Comparing the impedances in Fig. 12 and Fig. 13 to the three situations listed in Section II. which could imply a risk of SSCI, it is seen that the criteria for situation b) are fulfilled, since $R_{wtg} = -0.18\ \Omega$ when $X_{grid} = 0$ at about 11.5 Hz. The criteria for situation c) are also fulfilled, since $R_{sum} = -0.11\ \Omega$ when $X_{sum} = 0$ at about 10.6 Hz, and $R_{sum} = -26.54\ \Omega$ when $X_{sum} = 0$ at about 42 Hz (these are series resonance points, the parallel resonance points are not considered).

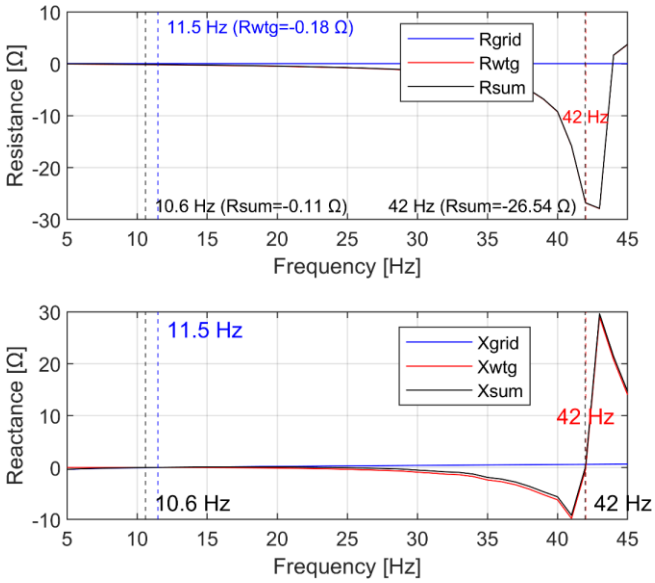

Fig. 12. Case A resistance and reactance (series resonance points only).

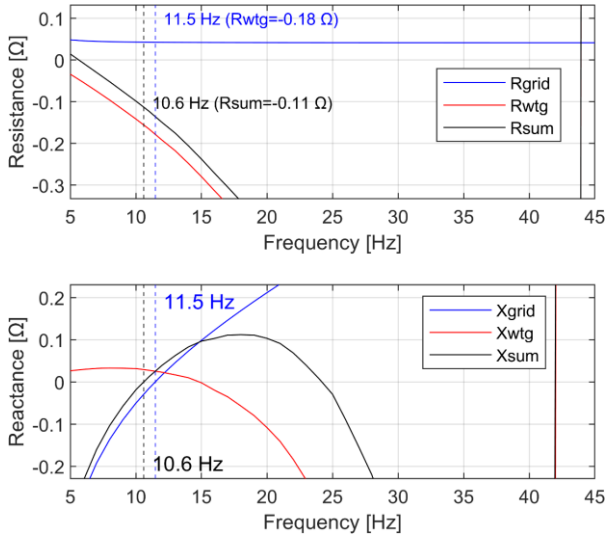

Fig. 13. Case A resistance and reactance zoomed in around the 10.6 Hz resonance point.

2) Nyquist Criterion

For the Nyquist criterion analysis, transfer functions of Z_{wtg} and Z_{grid} were used (Z_{wtg} being approximated by pole and zero placement). The poles and zeros of Z_{wtg}, Z_{grid} and $Z_{sum} = Z_{grid} + Z_{wtg}$ are seen in Fig. 14. The wind turbine and the grid only have stable poles and zeros (i.e., all are in the LHP), while the sum of the two transfer functions results in an unstable zero pair (i.e., in the RHP).

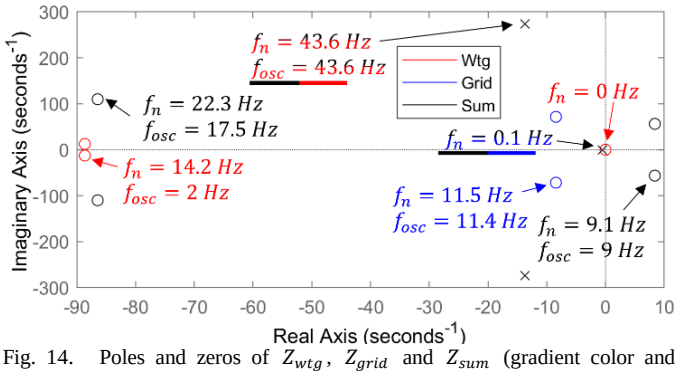

Fig. 14. Poles and zeros of Z_{wtg}, Z_{grid} and Z_{sum} (gradient color and underline mean pole/zero exists in multiple transfer functions).

The comparison between the measured Z_{sum} and the approximated version is seen in Fig. 15. The approximated transfer functions do not give an exact match with the measured data, but the match is deemed sufficient for the analysis.

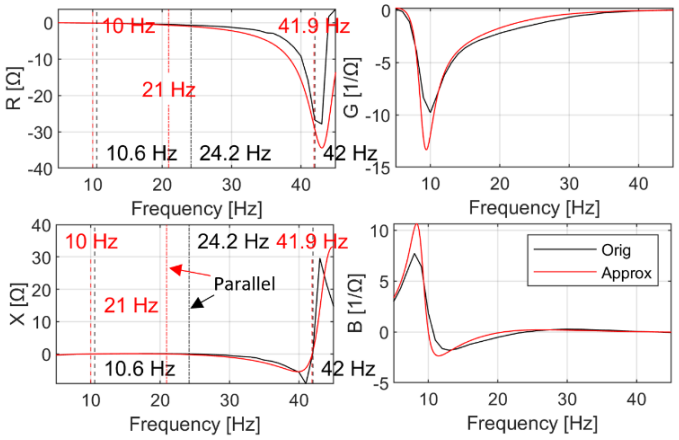

Fig. 15. Impedance and admittance of Case A sum (grid and wtg): measured (black) and approximated (red). Series and parallel resonances in dashed and dash-dotted line, respectively.

The Nyquist plot of the open-loop transfer function G_{OL} is seen in Fig. 16, where the measured is compared to the approximated. As described earlier, if G_{OL} is stable, G_{CL} is stable if $\Re(G_{OL}) > -1$ when $\Im(G_{OL}) = 0$. The open-loop G_{OL} is stable, since it has no poles (nor zeros) in the RHP (as seen in Fig. 17), meaning that the above condition can be used to assess stability. By observing Fig. 16 it is evident that the closed-loop G_{CL} is unstable since when $\Im(G_{OL}) = 0$, $\Re(G_{OL}) < -1$. The point $-1 + 0j$ lies to the right of the Nyquist plot, which also confirms an unstable G_{CL}.

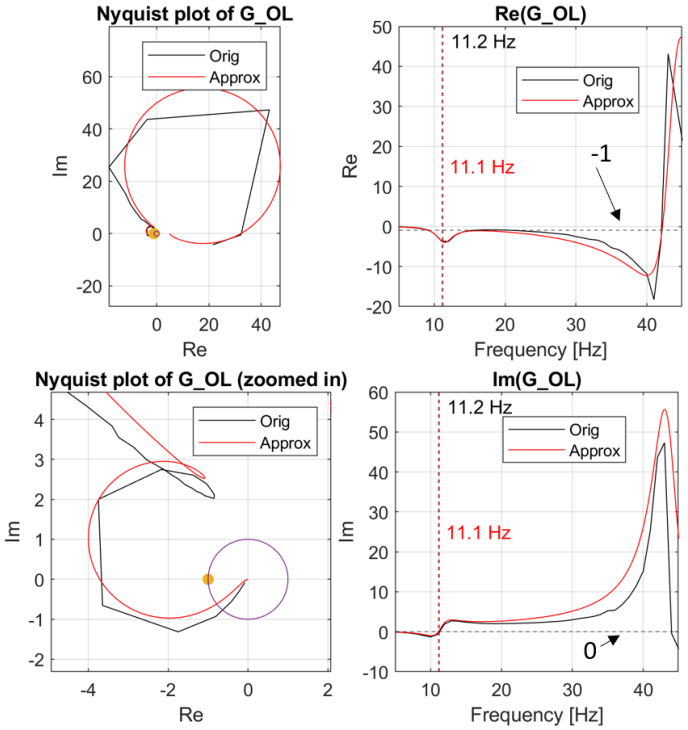

Fig. 16. Case A G_{OL} (the point $-1 + 0j$ marked with a yellow dot, and the unit circle with a purple circle). Zero crossing of $\Im(G_{OL})$ marked with dashed line.

The poles and zeros of G_{OL} and G_{CL} are seen in Fig. 17, where it is observed that there is an unstable pole pair in G_{CL} with a natural frequency of 9.1 Hz and an oscillatory frequency (imaginary part of pole) of 9 Hz. This unstable pole pair is the unstable zero pair seen in Z_{sum} in Fig. 14, and is explained by the fact that the denominator of G_{CL} is $Z_{grid} + Z_{wtg}$ as in (1), i.e., the zeros of Z_{sum} correspond to the poles of G_{CL}.

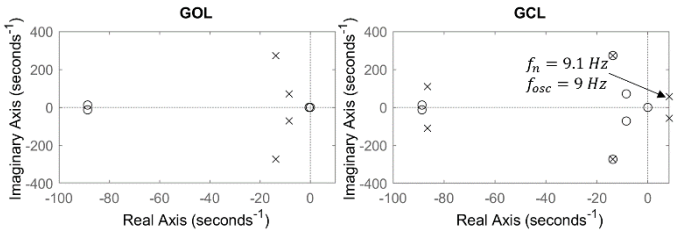

Fig. 17. Case A open-loop and closed-loop poles and zeros.

The natural and oscillatory frequency of the unstable closed-loop pole pair, as well as the reactance crossover frequencies (series resonance only) and the actual oscillating frequency (from the time domain simulation) are shown in TABLE I. The oscillatory frequency of the unstable G_{CL} pole pair corresponds well to the actual oscillatory frequency.

TABLE I
CASE A FREQUENCY COMPARISON

$f_{sum_{sr}}$ [Hz] (reactance crossover) (approx. value in parenthesis)	f_n of RHP pole in G_{CL} [Hz] (f_{osc} in parenthesis)	Actual f_{osc} [Hz]
10.6 (10), 42 (41.9)	9.1 (9)	8-9

B. Case B with 20% and 50% Compensation

1) Reactance Crossover Criteria

Using the reactance crossover method on the measured impedance of the wind farm, the grid, and the sum of the two for both 20% and 50% compensation degree gives the result seen in Fig. 18, with a zoomed-in y-axis. As in Case A, there is a series resonance at about 42 Hz which is not pointed out nor clearly observable in Fig. 18 due to it looking almost identical to the one in Case A (since the wind turbine impedance is dominating at those frequencies). The criteria for situation a) are not met for neither 20% nor 50% compensation degree, while the criteria for both situation b) and c) are met. Criteria for situation b) are met at 12.9 Hz and 20.8 Hz with 20% and 50% compensation, respectively, since $X_{grid} = 0$ and $R_{wtg} < 0$ at those frequencies. Criteria for situation c) are met at 12.6 Hz and 41.9 Hz with 20% compensation, and only at 42 Hz with 50% compensation, since $X_{sum} = 0$ and $R_{sum} < 0$ at those frequencies. In the 50% compensation case, the grid has a series resonance point at about 20.8 Hz, but when adding X_{grid} to X_{wtg}, the total reactance X_{sum} does not cross 0 around this frequency, but it is close (it is closest at about 22 Hz, and the corresponding resistance is negative).

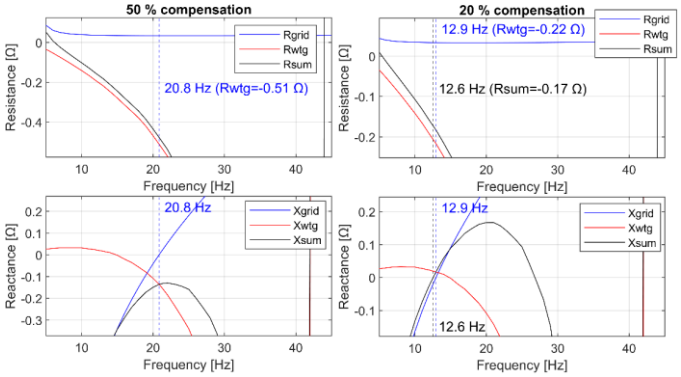

Fig. 18. Case B resistance and reactance zoomed in.

2) Nyquist Criterion

As in Case A, transfer functions of Z_{grid} and Z_{wtg} were used (the wind farm impedance is the same as in Case A). The measured and approximated Z_{sum} for both 20% and 50% compensation degree are compared in Fig. 19. Note that the y-axes of the resistance and reactance are zoomed in and that the resonance at about 42 Hz is therefore not clearly observable.

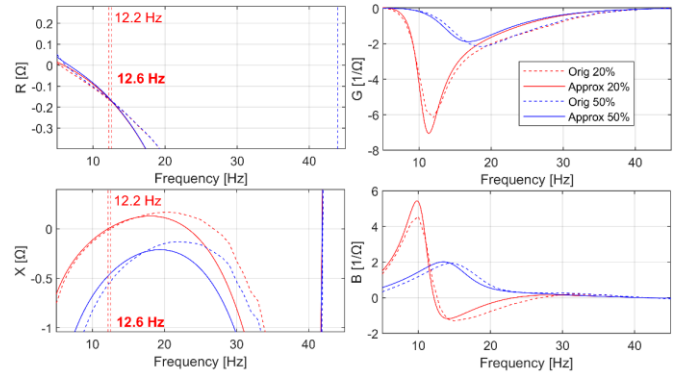

Fig. 19. Impedance and admittance of Case B sum (grid and wtg): 20% compensation (red) and 50% compensation (blue). Resonances shown with dashed vertical lines, with measured resonances in bold.

The poles and zeros of Z_{grid}, Z_{wtg}, and Z_{sum} are given in Fig. 20, where it is observed that Z_{sum} has an unstable zero pair with natural frequency 10.9 Hz and oscillatory frequency 10.7 Hz when the compensation degree is 20%, and an unstable zero pair with natural frequency 15.5 Hz and oscillatory frequency 14.8 Hz when the compensation degree is 50%.

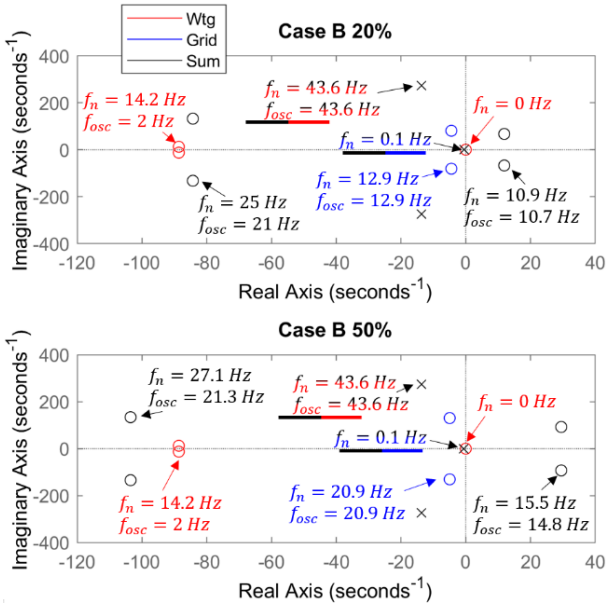

Fig. 20. Poles and zeros of Z_{wtg}, Z_{grid} and Z_{sum} (gradient color and underline mean pole/zero exists in multiple transfer functions).

The Nyquist plots of the measured G_{OL} for both 20% and 50% compensation are shown in Fig. 21, where a comparison to the approximated transfer functions is also given. It is observed that the Nyquist plot lies to the left of the point $-1 + 0j$, meaning an unstable G_{CL}, for both 20% and 50% compensation. The same conclusion is drawn by observing that when $\Im(G_{OL}) = 0$, $\Re(G_{OL}) < -1$.

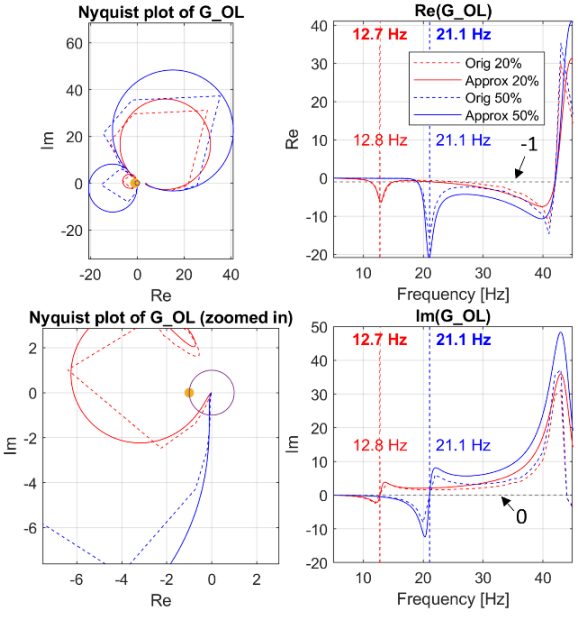

Fig. 21. Case B G_{OL} (the point $-1 + 0j$ marked with a yellow dot, and the unit circle with a purple circle). Zero crossing of $\Im(G_{OL})$ marked with dashed line. Measured zero crossing in bold.

The poles and zeros of G_{OL} and G_{CL} for 20% and 50% compensation are shown in Fig. 22, where it is observed that G_{OL} is stable, i.e., no RHP poles (nor zeros), for both compensation degrees. In G_{CL} there is an unstable pole pair with natural frequency 10.9 Hz and oscillation frequency 10.7 Hz for the 20% compensation degree, and with natural frequency 15.5 Hz and oscillation frequency 14.8 Hz for the 50% compensation degree. As in Case A, the oscillation frequency of the two unstable pole pairs matches the actual oscillation frequencies (from the time domain simulations) well.

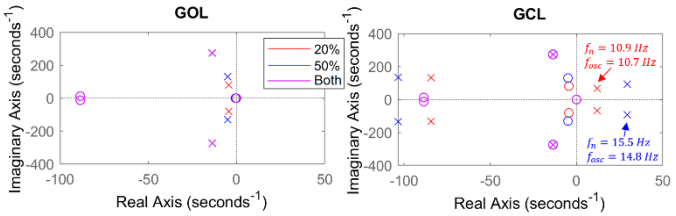

Fig. 22. Case B open-loop and closed-loop poles and zeros.

In TABLE II the natural and oscillatory frequency of the unstable closed-loop pole pairs, as well as the reactance crossover frequencies (series resonance only) and the actual oscillating frequency (from the time domain simulation) are listed.

TABLE II
CASE B FREQUENCY COMPARISON

Comp. degree	$f_{sum_{sr}}$ [Hz] (reactance crossover) (approx. value in parenthesis)	f_n of RHP pole in G_{CL} [Hz] (f_{osc} in parenthesis)	Actual f_{osc} [Hz]
20%	12.6 (12.2), 41.9 (41.9)	10.9 (10.7)	10-11
50%	Close to 0 at 22 Hz but not crossing, 42 (41.9)	15.5 (14.8)	15

VII. Discussion

This paper has presented three case studies of a DFIG wind farm connected to a series compensated system, with two of the case studies being modelled using line configurations typical in the Swedish transmission system, with different series compensation degrees. The impedance of the wind farm + grid has been analyzed for the situation where the two are radially connected, assessing the risk of SSCI. A PV farm was modelled and installed at the PCC of the wind farm, aiming to act as a PV-STATCOM to damp sub-synchronous oscillations.

Two methods were used for the SSCI risk assessment: the reactance crossover method, and the Nyquist criterion. The former method, consisting of three criteria, showed that the criteria for situation c) were met in all cases, since a series resonance point in Z_{sum} with $R_{sum} < 0$ at about 42 Hz was present in all cases. However, no oscillations at this frequency were observed in the time domain voltage or current waveforms. In Case A and Case B with 20% compensation, the criteria for situation c) were also met at 10.6 Hz and 12.6 Hz, respectively, where $X_{sum} = 0$ (series resonance only) and $R_{sum} < 0$. The oscillations in time domain (both in voltage and current) were of about 8-9 Hz and 10-11 Hz, respectively. It is worth noting that the apparent series resonance in Z_{sum} at 42 Hz is driven by the wind turbine, not by the grid, as opposed to the series resonance at lower frequencies. In Case B with 50% compensation, there were no other series resonance points (in Z_{sum}) except at 42 Hz, but in the time domain simulations there were undamped current and voltage oscillations of about 15 Hz. The criteria for situation b) were however met at about 20.8 Hz, so even though the reactance crossover method did not predict the oscillation frequency as precisely as in the other two cases, it still predicted instability.

The Nyquist criterion was applied to both the measured impedances and approximated analytical transfer functions. The approximated transfer function of the wind farm was found by pole and zero placement, attempting to use as few poles and zeros as possible while maintaining the basic shape of the impedance and admittance. Both the measured and approximated open-loop transfer functions confirmed an unstable closed-loop transfer function in all cases. The actual oscillation frequency (in both current and voltage, found by time domain simulations) matched the oscillation frequency of the unstable pole pair in G_{CL} well. It was observed that the zeros of $Z_{sum} = Z_{grid} + Z_{wtg}$ correspond to the poles of G_{CL}. This is closely connected to the reactance crossover criterion, but it is seen that $Z_{sum} = 0$ and $R_{sum} < 0$ does not necessarily mean that there will be undamped oscillation at that frequency. The reactance crossover criterion suggested sub-synchronous oscillations at about 42 Hz in all cases, but by analyzing the poles and zeros of Z_{sum} it was observed that this reactance crossover appears to be caused by a pole with natural frequency close to 42 Hz (i.e., a zero in G_{CL}, meaning it will not cause instability). Case B with 50% compensation had no series reactance crossover in Z_{sum} except the one at about 42 Hz, but it was close at about 22 Hz. The unstable pole pair in the corresponding G_{CL} had a larger negative damping than those in Case A and Case B with 20% compensation, meaning a bigger difference between natural frequency and oscillation frequency. This could explain why the (almost) reactance crossover at about 22 Hz differs more to the actual oscillation frequency compared to the other two cases.

The reactance crossover at about 42 Hz, appearing in all studied cases, is driven by the impedance of the turbine model. This model is a generic DFIG model created by Manitoba Hydro International, and there are differences to a manufacturer model. However, the conclusions made in this paper still hold since it was simply illustrated how the reactance crossover criterion can sometimes be misleading regarding oscillation frequency, but that by analyzing the poles and zeros the true instabilities can be found.

It should be noted that the analytical transfer function of the wind turbine was approximated based on a measured impedance between 5-45 Hz. The poles and zeros of Z_{wtg} might therefore change if the fit is made for a larger frequency range. The current fit could also have been improved further, but the focus was on matching the basic shape and not a complete fit, also due to the uncertainties in the measured impedance.

In all case studies, the PV farm was able to successfully damp the sub-synchronous oscillations by acting as a PV-STATCOM. It should be noted that the impedance of the PV farm was not taken into consideration, and that when it was

connected to the PCC, the resonance conditions may have been altered.

VIII. Conclusions

In this paper, the risk of SSCI due to a DFIG wind farm interacting with a series compensated grid was investigated using two methods: the reactance crossover method, and the Nyquist criterion. The former indicated that in some cases, there will be a series resonance of the combined wind farm and grid impedance at a frequency in the vicinity of the actual oscillation frequency. In other cases, however, there may be sub-synchronous oscillations without a reactance crossover (of the combined wind farm and grid impedance) in the vicinity of the frequency of the oscillation. The latter method showed that all studied cases were unstable, since the open-loop transfer functions were shown to encircle the point $-1 + 0j$, thus confirming unstable closed-loop transfer functions. Transfer functions of the measured impedances showed that in all cases, there was an unstable pole pair in the closed-loop transfer function with oscillatory frequency close to the actual oscillation frequency.

Furthermore, a PV farm was connected in parallel to the wind farm with the aim of damping sub-synchronous oscillations due to SSCI, which it succeeded in doing.

The main conclusion from this paper would be a recommendation to use both the reactance crossover method and the Nyquist criterion to assess the risk of SSCI. While exact results might not be obtained, these studies should be seen as a screening study. To verify, time-domain simulations should be performed.

IX. References

[1] 'Systemutvecklingsplan 2022-2031 - Vägen mot en dubblerad elanvändning'. Svenska kraftnät.

[2] 'Specific study requirements for power park modules connected in vicinity of Fingrid's series compensated network'. Fingrid, Jan. 07, 2021.

[3] G. D. Irwin, A. K. Jindal, and A. L. Isaacs, 'Sub-synchronous control interactions between type 3 wind turbines and series compensated AC transmission systems', in *2011 IEEE Power and Energy Society General Meeting*, San Diego, CA, Jul. 2011, pp. 1–6. doi: 10.1109/PES.2011.6039426.

[4] A. Elgaali, 'Sub-synchronous controller interaction (SSCI) of series-compensated DFIG wind farms', Master Thesis, Chalmers University of Technology, Sweden, 2016. Accessed: Jan. 18, 2022. [Online]. Available: https://hdl.handle.net/20.500.12380/248309

[5] I. Löfgren, 'Mitigating SSCI in a hybrid wind and PV farm utilizing PV-STATCOM: A Swedish case study', Master Thesis, Dalarna University, Borlänge, 2022. Accessed: Aug. 30, 2022. [Online]. Available: http://du.diva-portal.org/smash/record.jsf?pid=diva2%3A1690268

[6] B. Badrzadeh, M. Sahni, D. Muthumuni, Y. Zhou, and A. Gole, 'Sub-synchronous interaction in wind power plants - part I: Study tools and techniques', in *2012 IEEE Power and Energy Society General Meeting*, San Diego, CA, Jul. 2012, pp. 1–9. doi: 10.1109/PESGM.2012.6344894.

[7] B. Badrzadeh, M. Sahni, Y. Zhou, D. Muthumuni, and A. Gole, 'General Methodology for Analysis of Sub-Synchronous Interaction in Wind Power Plants', *IEEE Trans. Power Syst.*, vol. 28, no. 2, pp. 1858–1869, May 2013, doi: 10.1109/TPWRS.2012.2225850.

[8] U. Karaagac, J. Mahseredjian, S. Jensen, R. Gagnon, M. Fecteau, and I. Kocar, 'Safe Operation of DFIG-Based Wind Parks in Series-Compensated Systems', *IEEE Trans. Power Deliv.*, vol. 33, no. 2, pp. 709–718, Apr. 2018, doi: 10.1109/TPWRD.2017.2689792.

[9] S. Chernet and M. Bongiorno, 'Input impedance based nyquist stability criterion for subsynchronous resonance analysis in DFIG based wind farms', in *2015 IEEE Energy Conversion Congress and Exposition (ECCE)*, Montreal, QC, Canada, Sep. 2015, pp. 6285–6292. doi: 10.1109/ECCE.2015.7310541.

[10] L. Keviczky, R. Bars, J. Hetthéssy, and C. Bányász, *Control Engineering*. Singapore: Springer Singapore, 2019. doi: 10.1007/978-981-10-8297-9.

[11] 'Type 3 Wind Turbine Model (PSCAD v4.6)'. Manitoba Hydro International Ltd., 2018.

[12] 'Interface to Harmonic Impedance Solution (Frequency Scanner)', *PSCAD*. https://www.pscad.com/webhelp/Master_Library_Models/Meters/Harmonic_Impedance_Solution/harm_imp_int.htm (accessed Feb. 14, 2022).

[13] Huawei, 'SUN2000-215KTL-H0 Smart String Inverter'. Accessed: May 06, 2022. [Online]. Available: https://solar.huawei.com/en-GB/download?p=%2F-%2Fmedia%2FSolar%2Fattachment%2Fpdf%2Feu%2Fdatasheet%2FSUN2000-215KTL-H0.pdf